Preprint Title	Controlling the proximity in a Co/Nb multilayer: the properties of electronic transport
Authors	Sergey Bakurskiy, Mikhail Kupriyanov, Nikolay V. Klenov, Igor Soloviev, Andrey Schegolev, Roman Morari, Yury Khaydukov and Anatoli Sidorenko
Publication Date	05 Jun 2020
Article Type	Full Research Paper
ORCID® iDs	Mikhail Kupriyanov - https://orcid.org/0000-0003-1204-9664; Nikolay V. Klenov - https://orcid.org/0000-0001-6265-3670

Controlling the proximity in a Co/Nb multilayer: the properties of electronic transport

Sergey Bakurskiy[1], Mikhail Kupriyanov[1], Nikolay Klenov*[1-4], Igor Soloviev[1,4,5], Andrey Schegolev[2,3], Roman Morari[4,6], Yury Khaydukov[1,7], and Anatoli Sidorenko[6,8]

Address: [1]Lomonosov Moscow State University Skobeltsyn Institute of Nuclear Physics, Moscow, 119991, Russia; [2]Lomonosov Moscow State University Physics Department, Moscow, 119991, Russia; [3]Moscow Technical University of Communication and Informatics (MTUCI), 111024 Moscow, Russia; [4]Moscow Institute of Physics and Technology, State University, Dolgoprudny, Moscow Region 141700, Russia; [5]Lobachevsky State University of Nizhny Novgorod, Nizhny Novgorod 603950, Russia; [6]Institute of Electronic Engineering and Nanotechnologies ASM, MD2028 Kishinev, Moldova; [7]Max-Planck-Institut für Festkörperforschung, Heisenbergstraße 1, D-70569 Stuttgart, Germany; [8]Laboratory of Functional Nanostructures, Orel State University named after I.S. Turgenev, 302026, Russian Federation

Email: Nikolay V. Klenov – nvklenov@gmail.com

* Corresponding author

Abstract

We present both a theoretical and experimental investigation of the proximity effect in a stack-like superconductor/ferromagnet (S/F) superlattice, where ferromagnetic layers with different thicknesses and coercive fields are made of Co. Calculations based on Usadel equations allow us to find conditions at which switching from the

parallel to the antiparallel alignment of neighboring F-layers leads to a significant change of the superconducting order parameter in thin s-films. Experimentally we study the transport properties of a lithographically patterned Nb/Co multilayer. We observe that the resistive transition of the multilayer contains multiple steps, which we attribute to the transition of individual s-layers with T_c's depending on the local magnetization orientation of neighbor F-layers. We argue that such superlattices can be used as tunable kinetic inductors, designed for artificial neural networks with a representation of information in current domain.

Keywords

cryogenic computing; spin-valve; superconducting spintronics; superconducting neural network.

Introduction

Multilayer superconductor/ferromagnet (S/F) heterostructures can be used for construction of tunable cryolelctronic element, such as switches, Josephson junctions, inductances *et cetera* [1-8]. Below we present theoretical and experimental investigations of an S/F "stranded wire" with a controllable proximity effect. The wire is composed of ferromagnetic (F) layers separated by thin superconducting layers (s), in which the superconducting order parameter is supported due to the proximity to a thick superconducting S-bank. Switching from the antiparallel (AP) to the parallel (P) alignment of neighboring F_1 and F_2 layers leads to a significant enhancement of the effective exchange field in such an artificial ferromagnet. Previously, properties of [Co (1.5 nm) / Nb (8 nm) / Co (2.5 nm) / Nb (8 nm)]$_6$ multilayer structures for cryogenic memory applications were studied using neutron scattering and magnetometry techniques [9]. In particular, parameter regions where the

aforementioned switching between the P and AP orientations of the F_1 and F_2 layers is possible, was found experimentally.

In this work we perform theoretical and experimental analysis of electronic properties of Nb/Co multilayers with different F_1 and F_2 thicknesses and several stacking periods. It is demonstrated that magnetization switching result in modulations of superconductivity in the superlattice with a corresponding change in kinetic inductances of superconducting parts of the wire core, due to the inverse proximity effect. We argue that this effect facilitates new possibilities for development of tunable superconducting electronic components. For example, the considered “stranded wire” can be readily applied in a synaptic connection for a superconducting artificial neural networks (ANN) where information is represented in a “current domain” [10-21].

The paper is organized as follows. In the next Section we highlight the manifestation of the proximity effect in hybrid S/F structures, the most interesting for the applications discussed, present the model and methods of theoretical research, and formulate obtained results. In the Section “Experimental Results” we analyze the transport measurements of the manufactured samples. At the end, we discuss possible applications of the results for implementations of superconducting synapses and give a conclusion.

Model and theoretical results

Contrary to traditional semiconductor basic elements (transistors), the tunable kinetic inductors (TKI) as well as nonlinear elements (Josephson junctions) are not fabricated in a substrate. That allows benefiting from 3D topology, which is especially important for deep ANNs. The F_1/s/F_2/s super-lattice, in which the thick S-bank acts

as the source of induced superconductivity, is the simplest “model” of the 3D structure. Let us consider the applications, which are possible due to control over the order parameter in thin s-layers in such a structure.

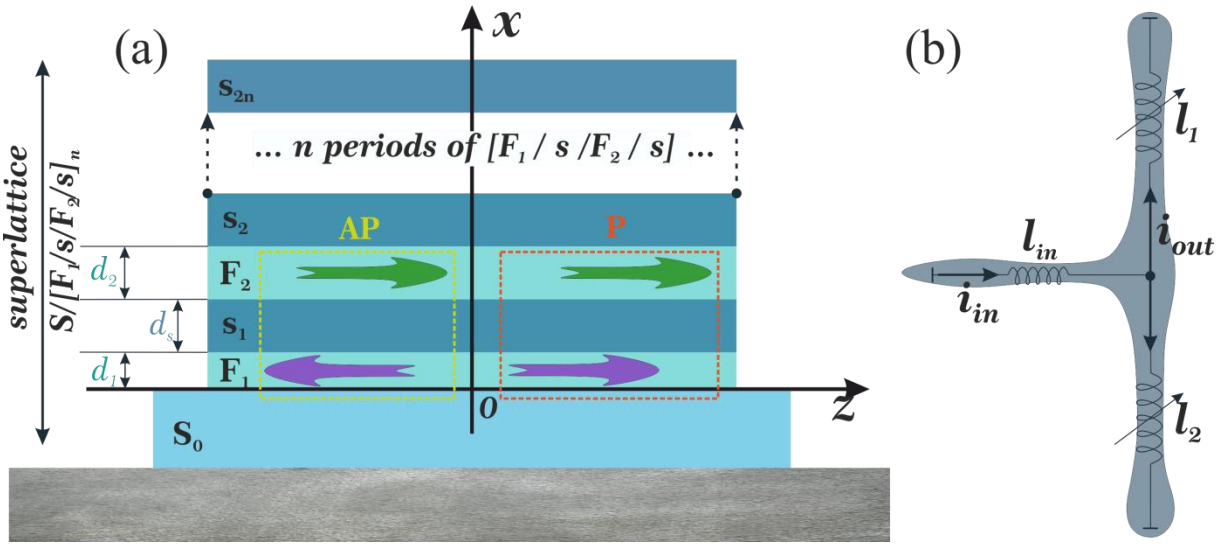

Figure 1: (a) Sketch of the investigated multilayer Co(1.5 nm)/Nb(6 nm)/Co(2.5 nm)/Nb(6 nm) structure. (b) The simplest splitter based on this TKIs.

The simplest cell for the current flow control using the TKI is a splitter. The input current, i_{in}, induced in the input inductance, l_{in}, splits toward the two TKI elements. Figure 1b presents the principal scheme of synaptic element in superconducting ANN (with TKI elements instead of Josephson junctions in [20]). The synapse modulates the “weight” of an arriving signal, which corresponds to the input current. The transfer function of such a current transformer can be described as follows:

$$i_{out} = i_{in} \cdot \frac{\Delta l}{\Sigma l + 2l_p} \qquad (1)$$

where i_{in} and i_{out} stands for the normalized input/output current respectively, $\Delta l = l_1 - l_2$; $\Sigma l = l_1 + l_2$; l_1, l_2 are the values of normalized inductance for two TKIs, lp is the stray geometric inductance of a splitter branch. For the functioning of the device, it is

critically important to find conditions when the kinetic inductance changes significantly due to the controlled proximity effect in the S/F structure.

To test the concept of the magnetically tunable kinetic inductor we calculated the superconducting order parameter in S/[F_1/s/F_2/s]$_n$ superlattices presented in Figure 1. We study proximity effect and electronic transport in the multilayer hybrid structures in the frame of Usadel equations [22]

$$\frac{\pi T_C \xi_p^2}{\widetilde{\omega}_p G_m}\frac{d}{dx}\left(G_p^2\frac{d\Phi_p}{dx}\right)-\Phi_p=-\Delta_p,\quad G_\omega=\frac{\widetilde{\omega}}{\sqrt{\widetilde{\omega}^2+\Phi_\omega\Phi^*_{-\omega}}} \tag{2}$$

$$\Delta_p\ln\frac{T}{T_C}+\frac{T}{T_C}\sum_{\omega=-\infty}^{\infty}\left(\frac{\Delta_p}{|\omega|}-\frac{\Phi_p G_p}{\omega}\right)=0,$$

with Kupriyanov-Lukichev boundary conditions [23, 24]

$$\pm\gamma_{Bpq}\xi_p G_p\frac{d}{dx}\Phi_p=G_q\left(\frac{\widetilde{\omega}_p}{\widetilde{\omega}_q}\Phi_q-\Phi_p\right), \tag{3}$$

at the SF interfaces. Here $G_{p,q}$ and $\Phi_{p,q}$ are normal and anomalous Green's functions, $\omega=\pi T(2n+1)$ is Matsubara frequency. $\widetilde{\omega}=\omega+iH$, where H is the exchange energy in F-layer, p and q – indexes, which denotes the materials, ξp – the coherence length, $\gamma_{Bpq}=R_{BA}/\rho_p\xi_p$ – interface parameter, where R_{BA} – the resistance per square of the interface and ρ_p – resistivity of material from the p-side of boundary. Note that the boundary conditions at the SF interface are written from the both sides, that leads to two independent parameters γ_{BSF} and γ_{BFS}. Their ratio $\gamma=\rho_S\xi_S/\rho_F\xi_F$ is suitable parameter for understanding the properties of the system, since it depends only from material properties.

In our calculations we put the origin of the x axis at free interface of the bulk S electrode with the thickness $L_S=10\xi_S$ and have considered its proximity effect with artificial ferromagnetic material (AFM) consisting of the alternating thin

superconducting (L_S =1 ξ_S) and ferromagnetic layers with exchange energy H=10T_C. In AFM every odd F layer has thickness L_{F1}=0.15 ξ_S, while every even ferromagnetic layer has thickness L_{F2}=0.1ξ_S. We assume that the diffusive coherence length of S and F material are the same, but relative resistivities can differ. Numerical solution of the boundary problem (2)-(3) provides the required spatial distribution of pair potential Δ(x) as well as anomalous Φ(x) and normal G(x) Green function for a given temperature.

We have found that behavior of the system significantly depends on the relative resistivities and coherence lengths of the chosen material. In the case γ=1, when ferromagnetic metal and superconductor have the same resistivity and diffusion coefficient, the pair potential in the whole structure evenly grows with decrease of the temperature (See Figure 2a). The main source of the superconductivity is the bulk S layer, while the thin s-layers just slightly support the pairing amplitude coming from the source. Figure 2b gives the spatial distributions of the anomalous Green function

$$F_\omega = \frac{\Phi_\omega}{\sqrt{\widetilde{\omega}^2 + \Phi_\omega \Phi^*_{-\omega}}}$$

at the first (n=0) Matsubara frequency, F_1, for parallel (solid line) and antiparallel (dashed) orientations of magnetization at small, T=0.25T_C (panel b), and large, T=0.6 T_C (panel c), temperatures. It is seen that the real part of F_1 decreases inside of AFM almost exponentially with small step-like modulation in thin superconducting layers. In the antiparallel case (AP) the decrease of the real part of functions versus coordinate is going slower with increase of x. At the same time, imaginary part behaves differently for P and AP configuration. In AP case imaginary part oscillates, returning almost to zero after every second layer. In P case imaginary part decreases almost exponentially, but slower than the real one, providing possibility of 0-π transition.

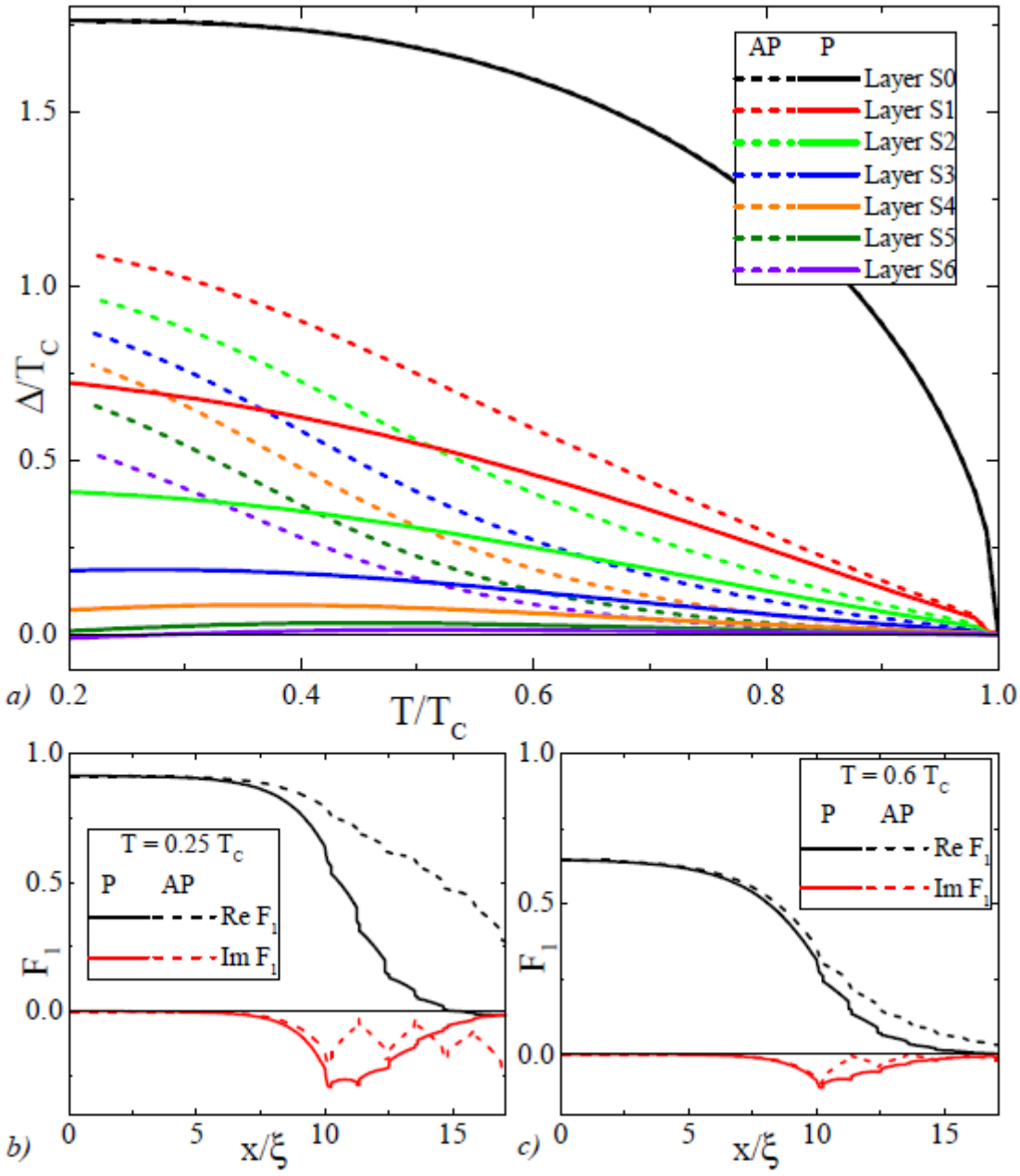

Figure 2: (a) Pair amplitude Δ in $S(F_1sF_2s)_{x3}F_1$ structure in different superconducting layers versus temperature T for parallel (solid lines) and antiparallel (dashed lines) orientations of magnetization for material parameter γ=1. (b,c) Spatial distributions of the anomalous Green function F_1 for parallel (solid lines) and antiparallel (dashed lines) orientation of magnetization at different temperatures: T=0.25T_C (b) and T=0.6T_C (c).

However, the properties of proximity effect are completely different if the resistivity of superconductor is significantly smaller than ferromagnetic one (γ=0.1*).* In this case, thin s-layer are protected from superconductivity suppression due to inverse proximity effect and the sF-multylayer acts as additional source of superconductivity. However, the effective critical temperature of that magnetic superconductor is significantly smaller than in the bulk S material. This property of the system is demonstrated in Fig 3. The panel (a) in Fig 3. presents the temperature dependencies of pair potential in different superconducting layers for the cases of P (solid lines) and AP (dashed) configurations of the magnetizations in F-layers. In the large S-electrode, the temperature dependence of pair potential coincides with prediction of pure BCS model. At the same time, the pair potential in thin s-layers rapidly arises near effective critical temperature T_C*~0.5T_C. It should be noticed, that the support of superconductivity from the bulk S source provides untrivial shape of $\Delta(T)$ in the closest s-layer with rapid jump of pair potential to a constant value in the vicinity of T_C*. The farther the layer is, the weaker the effect of support. Far s-layers has almost no impact from the bulk source and their properties are similar with independent $(sF)_x$ multilayer with sloping $\Delta(T)$ dependence.

The spatial distributions of Green functions (See Fig.3b,c) also have a step-like shapes. Since the pair potential inside the multilayer has independent superconducting source from the bulk S-layer, the value of the pairing amplitude F_1 is almost permanent inside every s-layer. However, this value inside each layer is strongly dependent from the distance from bulk electrode. At the temperature above T_C*, spatial distribution has similar shape, but the significant pairing amplitude appears only in the s-layers closest to the bulk S-electrode. The additional possible consequence of such spatial distribution appears in the screening of F-layers in multilayers from outer magnetic field due to Meissner effect. The inner F-layers are

screened strong, while outer layers are screened weaker. It means, that the remagnitization of the layers in increasing homogeneous external magnetic field doesn't occur simultaneously, but step by step: from outer to inner layers of the structure.

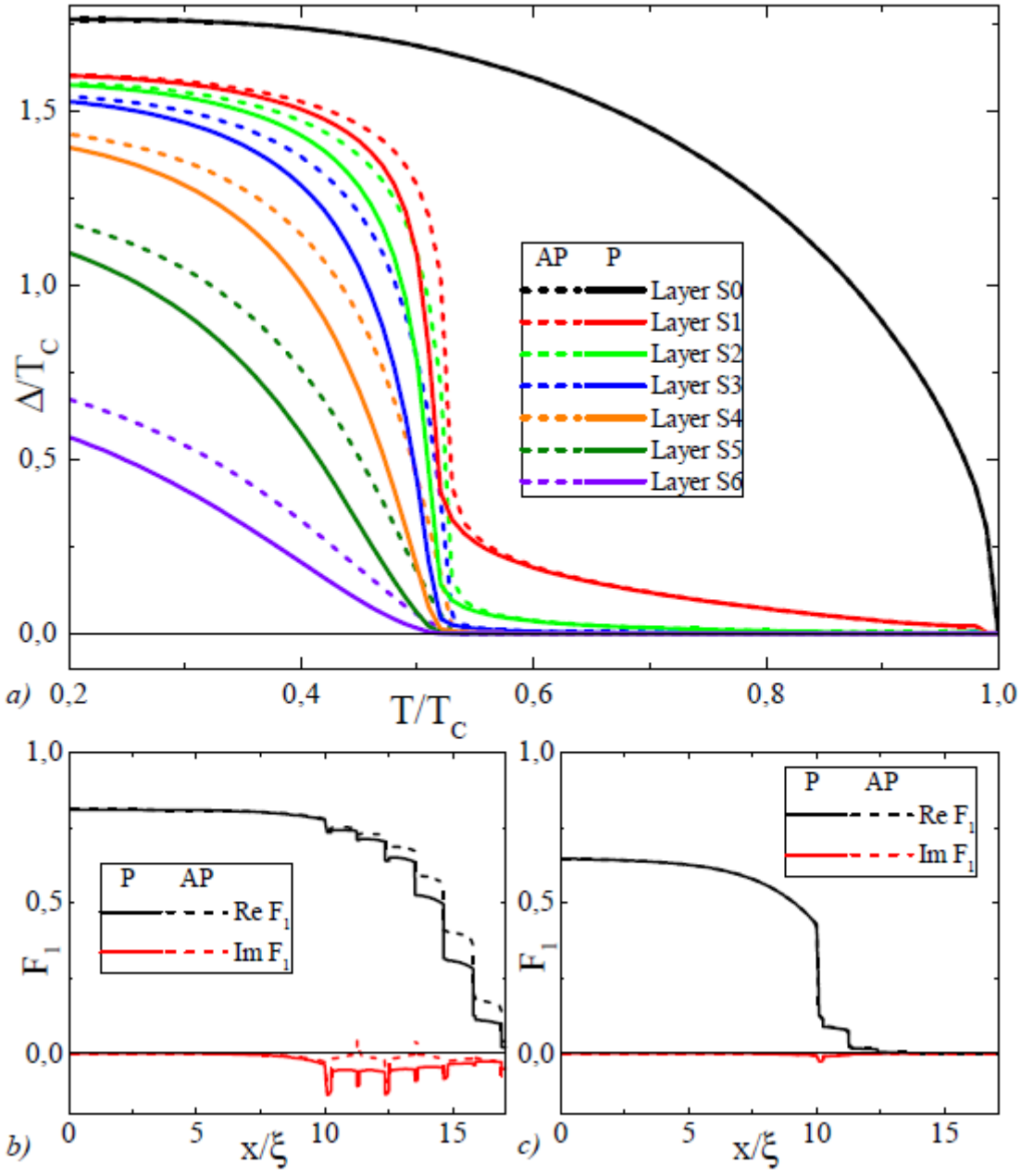

Figure 3: (a) Pair amplitude Δ in $S(F_1sF_2s)_{x3}F_1$ structure in different superconducting layers versus temperature *T* for parallel (solid lines) and antiparallel (dashed lines) orientation of magnetization for material parameter *γ*=0.1. (b,c) Spatial distributions of the anomalous Green function, *F*, for parallel (solid lines) and antiparallel (dashed

lines) orientation of magnetization at different temperatures: T=0.4T_C (b) and T=0.6T_C (c).

The calculated distribution of the anomalous Green function, F, permits to estimate the screening properties of the hybrid structure. The spatial distribution of the screening length directly depends on the proximization of the superconducting order parameter in the system [25]:

$$\lambda(x)^{-2} = \frac{16\pi T^2}{\rho} \sum_{\omega>0} Re(F(x)^2) \quad .$$

Hence, the screening length and kinetic inductance of the considered s-layers are significantly larger in the P case compared with the AP case. It leads to redistribution of the current flowing along the multilayer and increase the total kinetic inductance of the structure [26]

$$L_K \approx \mu_0 \frac{l}{W} \left[\int_0^d \lambda(x)^2 dx \right]^{-1} \quad ,$$

where l is length of the strip, W – width, and d is the thickness of multilayer. It can be concluded that small changes in temperature or applied magnetic field [9] can significantly change (from zero to relatively large values) the kinetic inductance of thin s-layers in the hybrid structures under consideration.

Experimental results

The next important step was to search for evidence of a significant changes in the pair potential in thin s-layers in [Co (1.5 nm) / Nb (8 nm) / Co (2.5 nm) / Nb (8 nm)]$_3$ AFM. For these superlattices the possibility of switching between P and AP cases

using magnetic fields with a strength of about 30 Oersteds has already been demonstrated [9]. The samples were prepared using magnetron sputtering system Leybold Herraeus Z-400 during single deposition cycle without depressurization the chamber. Only three targets were used for structure preparation: niobium (99.95% purity) as a superconducting Cooper pair generator and interlayer separator between two neighboring films of ferromagnetic layers grown using cobalt (99.95% purity); the pure silicon target (99.999%) was used to create a passivating layer to prevent structure oxidation. In details the deposition technology is described in [27].

The structure for transport measurements was etched in pure argon atmosphere (Ar^+ milling) in a CRYO RIE Alba Nova machine (Stockholm University). The pattern design allows to perform a four point type measurement of six segments of the sample in one cooling cycle (see Figure 4): the pair of contacts was applied for setting current and the pair of micro-wires – for an induced potential difference testing. All low-temperature measurements during this work were done using cryogen-free magnet system with a flowing gas insert.

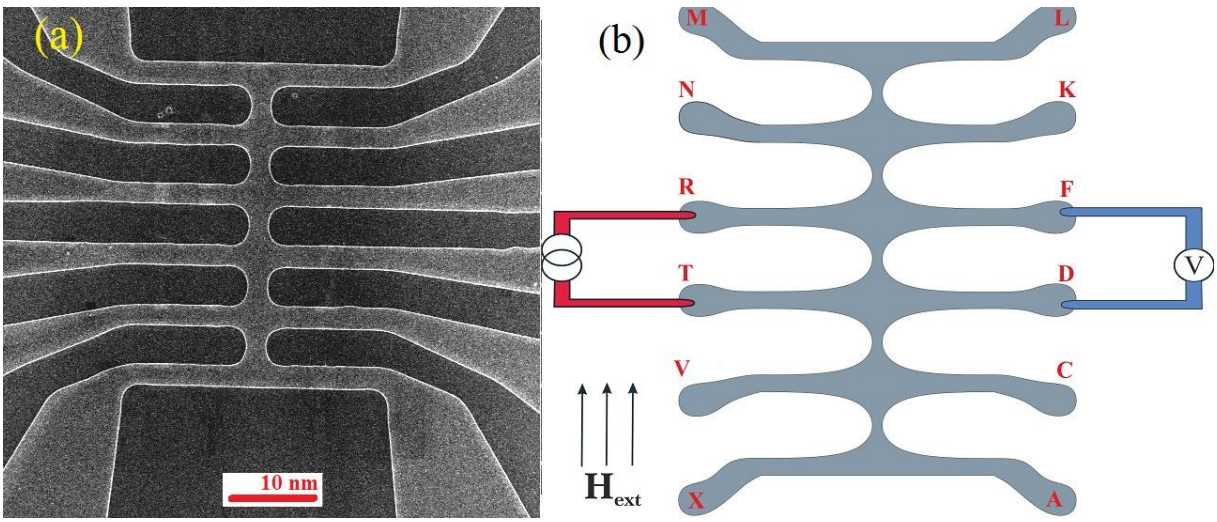

Figure 4: The microphotograph (a) and the principal scheme (b) of the structure fir critical temperature measurements.

The Figure 4 represents the principle scheme of measurement, this “centipede”-like sample design permits to measure electrical resistance of different “belly” (synapse-like) segments simply by alternating arms. The sample was cooled down to 10K in zero field cooling mode and no current was applied. Critical temperature measurements were started at 10 K by sweeping the temperature (R(T) measurements), and external 1μA current was used in AC mode with frequency 127Hz. The temperature change rate was chosen to provide minimal gradient for two cases – downward and upward sweep direction, and resulting shapes of curves totally resembled each other but slightly shifted by 0.05 K.

In this article we present only the results of three segments measurement because the rest demonstrated the similar behavior to either one of showed here. At the beginning the resistivity as function of temperature was measured without applied external magnetic field for all “belly” segments immediately after cooling down the sample. In Figure 5a we present R(T) curves for virgin case under zero applied field which correspond to common homogeneous superconductors measured in the same conditions: slight change of resistance above critical temperature and sharp unmistakable drop to zero in critical temperature region at 7.3K. The niobium falls to superconducting state throughout the entire volume of sample.The uppercase letters mean voltmeter contact connection on the principal scheme of sample (see Figure 4b), the current was applied to the opposite paths of the “centipede”. Note that in that initial state with random distribution of small domains in Co layers, resistive transitions $R(T)$ at different segments RT (black circles), TV (blue dashed line) and NR (red solid line) are similar in shape. The difference in resistances can be explained by geometrical factors (widths and particular shapes of the segments).

Next series of measurements were carried out under the same conditions but after training of sample in external magnetic field: the sample was exposed to alternating

magnetization in field applied parallel to layers of sample at 10K temperature. The magnetic field range was from -200 Oe to +200 Oe, during this process the electric current wasn't applied to the sample. After the remagnetization the $R(T)$ behavior significantly changes. For all segments the superconducting transition starts at a lower temperature T=7.2K and resistance gradually decreases until T=6.7K where it goes to zero. Moreover, several distinct steps appear in $R(T)$ curves, which we attribute to resistive transitions of individual superconducting layers, or groups of layers, in the multilayer. As explained in simulations above (see Figures 2 and 3), the effective critical temperature of s-layers within the multilayer, i.e., T at which the superconducting order parameter exceeds the value sufficient for carrying the applied transport current, depends on orientation of magnetizations in neighbor F-layers. It is at maximum for AP and at minimum for P orientation. From Figure 5 (b) o9ne can see that different segments may have a different sequence of steps. For example, segments RT (black circles) and TV (red line) have very similar $R(T)$ with three steps in the range 6.95 K < T < 7.05 K, while for a segment NR (blue dashed line) the steps have different shape and expand down to T = 6.7 K. This variation indicates that although the state of the multilayer is not homogeneous within the whole sample, it is still homogeneous enough within each segment to cause a significant variation of effective T_c's of individual layers with minimal values, corresponding to the P state.

Such behavior of $R(T)$ in the vicinity of T=7.3 is similar with dependencies of $R(T)$ in S/N and S/F contacts with conversion of normal to supercurrent. Furthermore, there are several jumps of resistance in the vicinity of temperature T=6.7K. The actual number of jumps changes for different electrodes (see Figure 5b).

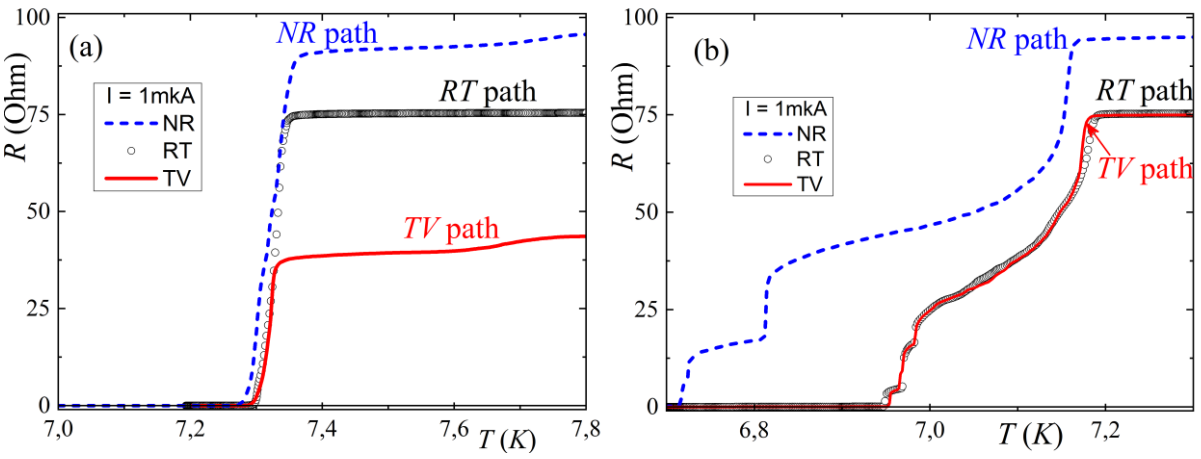

Figure 5: Dependence of the resistance versus temperature (a) without initial magnetization of the sample at current *I*=20mkA, and (b) after remagnetization in longitudinal direction at current *I*=1mkA.

The observed variation of step-like *R*(*T*) dependence may also be due to the specific sample geometry with different orientation of electrodes, horizontal or vertical in Figure 4(a). Due to the shape anisotropy, the “body” of the “centipede” is magnetized in longitudinal direction, while the arms are perpendicular to the field. Such geometry provides different magnetic structure and effective exchange field for different parts of the structure. It seems, that critical temperature of the arms is lower, than in the body, providing the injection of normal current into it, with conversion process inside it. It provides the finite voltage, measured on middle segments. At the same time, decrease of the temperature leads to transition of thin s-layers into superconducting state, which occurs step-by-step according to Figure 3 providing jumps on *R*(*T*) dependence.

This model is supported by results of our measurements: the resistance-temperature dependencies with current transport along *RT*- and *TV*-paths in Figure 5(b) are almost the same. It means, that the source of the voltage is in the *T*-electrode, which is the source of normal quasiparticles. At the same time, connection between *N* and

R electrodes provides the jumps at significantly smaller temperatures, which probably correspond to magnetic configuration in the *N* electrode.

Discussion and Conclusion

We continued theoretical and experimental research of Co/Nb multilayer, since neutron reflectometry and SQUID-magnetometry have proven that effective exchange energy can be controlled here by applying relatively weak magnetic fields. This time we focused on the "life" of superconductivity (pair potential) in thin s-layers in a changing "magnetic environment".

Theoretical studies in the present article have shown that it is possible to change "magnetically" the kinetic inductance of superconducting layers, and even transfer thin layers to a normal state at a fixed temperature.

Experimental studies have shown that transition of thin s-layers to the normal state in the considered multilayer structure is possible; the temperature of this transition depends on the magnetic environment.

Summarizing the entire above one can conclude that the electronic transport properties found in multilayer structure S/[F1/s/F2/s]n can be used to create different switching electronic elements, including synapses. Let's discuss this new type of application in more detail.

The creation of artificial neural networks is one of the current trends in the development of superconductor electronics [10-15]. Such an artificial neural network contains layers of elements that nonlinearly transform the incoming signal (neurons) connected by linear tunable connections (synapses). The number of synapses in neural networks that are interesting for applications is more than 10^6. Energy

dissipation at such interconnects is a serious problem, that explains the above-mentioned interest in energy-efficient superconducting solutions in this research field.

In the early 1990s, two-contact interferometers and their modifications operating in a resistive mode were used as basic elements (artificial neurons) in superconducting ANN. In such neurons, the signal level usually corresponded to the average voltage level in the cell. As a result, these ANN schemes were neither fast nor energy-efficient. The resumption of works in this area appeared at the end of the 2000s. This revival was associated with spike neural networks, in which information is presented as a sequence of identical (single-quantum) voltage pulses, and the signal corresponds to a time delay between pulses [10, 21]. From the point of view of circuitry, such neural networks resemble rapid single-flux-quantum (RSFQ) logic devices. But the development of energy-efficient modernization of the RSFQ logic forced us to look for the implementation of neural networks (and primarily synapses) with ultra-small energy dissipation. That was done based on adiabatic superconducting logic cells with the presentation of information in the form of magnitudes and directions of currents in superconducting circuits [17-19].

The main problem in these approaches is the complexity of the practical implementation of effective synaptic connections: they should be tunable but at the same time with memory effect. Recently, to create a synapse, it was proposed to use a Josephson contact with a ferromagnetic component in the weak coupling region, which makes it possible to adjust its critical current during the functioning of a neural network [20].

In this paper, we propose a way to completely eliminate a Josephson nonlinearity from the synapse circuit. The processes of switching on and off superconductivity in thin s-layers surrounded by magnetic materials can be used to to vary the transmission coefficient of the simplest synapse shown in Figure 1a. The

dependence of the output current i_{out} of the inductive synapse on the parasitic inductance, *lp*, and the sum of the controlled kinetic inductors of the arms, Σ*l* , is presented below. The configurable dynamic range of the element increases with the difference between the kinetic inductances of the arms and decreases with the rise of the geometric inductance.

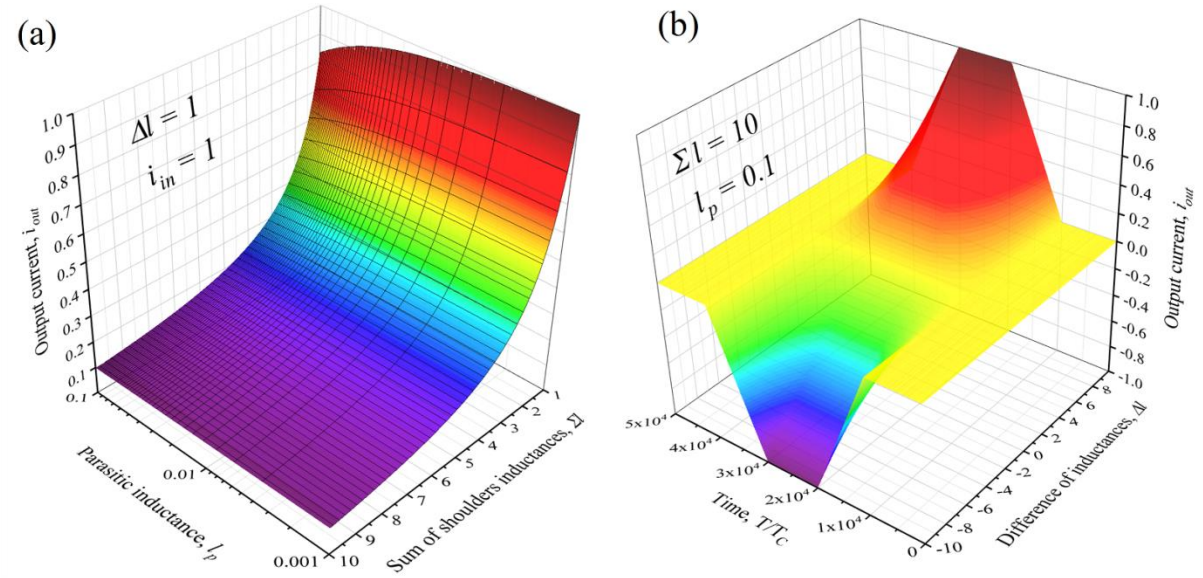

Figure 6: (a) Output current i_{out} of the inductive synapse versus the geometric inductance, *lp*, and the sum of the controlled kinetic inductors of the arms, Σ*l* .
(b) Output current under the action of a single input pulse for different values of the difference between the inductors of the arms, Δ*l*.

Taking into account more complex physical phenomena in the S/F multilayer the future studies promises to increase the functionality of the proposed synapse. With noncollinear magnetization in neighboring Co layers, the formation of a “long triplet” component in supercurrent is possible in the considered AFM [27-30]. This allows one to significantly influence on the magnitude of the order parameter in superconducting layers, controlling the misorientation angle of the magnetizations. The triplet superconducting correlations of electrons are formed from singlet correlations. Hence this effect reduces the kinetic inductance of the s-layers in a

quasi-monotonic manner with the value of the controlling magnetic field. This effect allows constructing the magnetically tunable kinetic inductor for artificial neural networks.

Acknowledgements

We are grateful to Vladimir Krasnov, Olena Kapran, Taras Golod, Vladimir Boian for sample fabrication and stimulating discussions. We acknowledge partial financial support of the Russian Science Foundation, Grant No. 20-69-47013 of the Russian Science Foundation (theoretical approach and calculations), R.M. is grateful for support of the Russian Ministry of Education and Science within the program 5top100. A.S. would like to thank the support of the European Union H2020-WIDESPREAD-05-2017-Twinning program ("SPINTECH" project under the grant agreement Nr. 810144). The samples were made in IEEN with the analytical support of the group from Orel State University. Neutron reflectometry is performed at the Max-Planck-Institut. The lithography was made at the Stockholm University.

References

1. Baek, B.; Rippard, W. H.; Benz, S. P.; Russek, S. E.; Dresselhaus, P. D. *Nat. Commun.* **2014,** *5,* 3888. doi:10.1038/ncomms4888

2. Alidoust, M.; Halterman, K. *Phys. Rev. B* **2014,** *89,* 195111. doi:10.1103/physrevb.89.195111

3. Gingrich, E. C.; Niedzielski, B. M.; Glick, J. A.; Wang, Y.; Miller, D. L.; Loloee, R.; Pratt Jr, W. P.; Birge, N. O. *Nat. Phys.* **2016,** *12,* 564–567. doi:10.1038/nphys3681

4. Shafranjuk, S.; Nevirkovets, I. P.; Mukhanov, O. A.; Ketterson, J. B. *Phys. Rev. Appl.* **2016,** *6,* 024018. doi:10.1103/physrevapplied.6.024018

5. Soloviev, I. I.; Klenov, N. V.; Bakurskiy, S. V.; Kupriyanov, M. Y.; Gudkov, A. L.; Sidorenko, A. S. *Beilstein J. Nanotechnol.* **2017,** *8,* 2689–2710. doi:10.3762/bjnano.8.269

6. Shafraniuk, S.E.; Nevirkovets, I.P.; Mukhanov, O.A. *Phys. Rev. Applied* **2019**, *11*, 064018. https://doi.org/10.1103/PhysRevApplied.11.064018

7. Golod, T.; Kapran, O.M.; Krasnov, V.M. *Phys. Rev. Applied* **2019**, *11*, 014062. doi: 10.1103/PhysRevApplied.11.014062

8. Satchell, N.; Shepley, P.M.; Algarni, M. *Appl. Phys. Lett.* **2020**, *116*, 022601. doi: 10.1063/1.5140095

9. Klenov N.; Khaydukov Y.; Bakurskiy S.; Morari R.; Soloviev I.; Boian V.; Keller T.; Kupriyanov M.; Sidorenko A.; Keimer B. Beilstein J. Nanotechnol. 2019, 10, 833–839. doi:10.3762/bjnano.10.83

10. Schneider, M. L; Donnelly, C. A.; Russek, S. E. *J. Appl. Phys.* **2018,** *124,* 161102.

11. Harada, Y.; Goto, E. *IEEE Trans, Magn.* **1991**, *27*, 2863.

12. Hidaka, M.; Akers, L. A. *Supercond. Sci, Technol.* **1991**, *4*, 654.

13. Mizugaki, Y.; Nakajima, K.; Sawada, Y.; Yamashita, T. *Appl. Phys. Lett.* **1993**, *62*, 762.

14. Mizugaki, Y.; Nakajima, K.; Sawada, Y.; Yamashita, T. *IEEE Trans. Appl. Supercond.* **1994**, *4*, 1.

15. Crotty, P.; Schult, D.; Segall, K. *Phys. Rev. E* 2010, *82*, 011914.

16. Chiarello, F.; Carelli, P.; Castellano, M. G.; Torrioli, G. *Supercond. Sci. Technol.* **2013**, *26*, 125009.

17. Yamanashi, Y.; Umeda, K.; Yoshikawa, N. *IEEE Trans. Appl. Supercond.* **2013**, *23*, 1701004.

18. Schegolev, A. E.; Klenov, N. V.; Soloviev, I. I.; Tereshonok, M. V. *Beilstein J. Nanotechnol.* **2016,** *7,* 1397–1403. doi:10.3762/bjnano.7.130

19. Klenov, N. V.; Schegolev, A. E.; Soloviev, I. I.; Bakurskiy, S. V.; Tereshonok, M. V. *IEEE Trans. Appl. Supercond.* **2018**, *28*, 1301006. http://dx.doi.org/10.1109/TASC.2018.2836903

20. Soloviev, I. I.; Schegolev, A. E.; Klenov, N. V.; Bakurskiy, S. V.; Kupriyanov, M. Y.; Tereshonok, M. V.; Shadrin, A. V.; Stolyarov, V. S.; Golubov, A. A. *J. Appl. Phys.* **2018,** *124,* 152113. doi:10.1063/1.5042147

21. Schneider, M. L.; Donnelly, C. A.; Russek, S. E.; Baek, B.; Pufall, M. R.; Hopkins, P. F.; Dresselhaus, P. D.; Benz, S. P.; Rippard, W. H. *Sci. Adv.* **2018**, *4*, e1701329.

22. Usadel, K. D. *Phys. Rev. Lett.* **1970,** *25,* 507–509. doi:10.1103/physrevlett.25.507

23. Kuprianov, M. Y.; Lukichev, V. F. *Sov. Phys. JETP* **1988** *67*, 1163-1168.

24. Bakurskiy, S. V.; Kupriyanov, M. Y.; Baranov, A. A.; Golubov, A. A.; Klenov, N. V.; Soloviev, I. I. *JETP Lett.* **2015,** *102,* 586–593. doi:10.1134/s0021364015210043

25. Mironov, S.; Mel'nikov, A. S.; Buzdin, A. *Appl. Phys. Lett.* **2018,** *113*, 022601.

26. Annunziata, A. J. *Single-photon detection, kinetic inductance, and non-equilibrium dynamics in niobium and niobium nitride superconducting nanowires*. – Yale University, 2010.

27. Morari, R.; Zdravkov, V.; Antropov, E.; Sidorenko, A.; J*. Nanoelectron. Optoelectron.* **2012***,* 7 () 678–680. https://doi.org/10.1166/jno.2012.1417.

28. Bergeret, F. S.; Volkov, A. F.; Efetov, K. B. *Phys. Rev. Lett.* **2001**, *86*, 3140. doi:10.1103/PhysRevLett.86.3140

29. Houzet, M.; Buzdin, A. I. *Phys. Rev. B* **2007**, *76*, 060504. doi:10.1103/PhysRevB.76.060504

30. Niedzielski, B. M.; Diesch, S. G.; Gingrich, E. C.; Wang, Y.; Loloee, R.; Pratt, W. P., Jr.; Birge, N. O. *IEEE Trans. Appl. Supercond.* **2014**, *24*, 1800307. doi:10.1109/TASC.2014.2311442

31. Zdravkov, V. I.; Lenk, D.; Morari, R.; Ullrich, A.; Obermeier, G.; Müller, C.; Krug von Nidda, H.-A.; Sidorenko, A. S.; Horn, S.; Tidecks, R.; Tagirov, L. R. *Appl. Phys. Lett.* **2013**, *103*, 062604. doi:10.1063/1.4818266